European Journal of Radiology 119 (2019) 108635

Contents lists available at ScienceDirect

European Journal of Radiology

journal homepage: www.elsevier.com/locate/ejrad

Research article

# Intravoxel incoherent motion (IVIM) for response assessment in patients with osteosarcoma undergoing neoadjuvant chemotherapy

Esha Baidya Kayal[a], Devasenathipathy Kandasamy[b], Kedar Khare[c], Sameer Bakhshi[d], Raju Sharma[b], Amit Mehndiratta[a,e,*]

[a] Centre for Biomedical Engineering, Indian Institute of Technology Delhi, New Delhi, India
[b] Department of Radiology, All India Institute of Medical Sciences, New Delhi, India
[c] Department of Physics, Indian Institute of Technology Delhi, New Delhi, India
[d] Department of Medical Oncology, Dr. B.R. Ambedkar Institute-Rotary Cancer Hospital (IRCH), All India Institute of Medical Sciences, New Delhi, India
[e] Department of Biomedical Engineering, All India Institute of Medical Sciences, New Delhi, India

ARTICLE INFO

*Keywords:*
Intravoxel incoherent motion (IVIM) diffusion weighted MRI analysis
Diffusion weighted imaging (DWI)
Imaging biomarkers for therapeutic response evaluation
Chemotherapy response evaluation
Bone tumor - osteosarcoma

ABSTRACT

*Purpose:* To explore the role of quantitative Intravoxel incoherent motion (IVIM) parameters and their histogram analysis in characterizing changes in Osteosarcoma receiving neoadjuvant chemotherapy (NACT) and evaluating therapeutic response.

*Methods:* Forty patients (N = 40; Male:Female = 30:10; Age = 17.7 ± 5.9years; Metastatic:localized = 17:23) with histologically confirmed Osteosarcoma treated with 3-cycles of NACT were analyzed prospectively. All patients underwent Diffusion weighted imaging (DWI) with 11 b-values (0–800 s/mm$^2$) using 1.5 T MRI scanner at pre-treatment (t0), after 1-cycle (t1) and after 3-cycles (t2) of NACT. Non-invasive response evaluation of NACT was performed using RECIST1.1 criteria. Apparent-diffusion-coefficient *(ADC)* and IVIM parameters – Diffusion-coefficient *(D)*, Perfusion-coefficient (*D**) & Perfusion-fraction (*f*) and their relative percentage changes from time-point t0–t1 (Δ2) and t0–t2 (Δ2) were evaluated and histogram analysis was performed at three time-points and compared with respect to RECIST1.1 scores.

*Results:* Using RECIST1.1 criteria, 11 (27.5%), 21 (52.5%) and 8 (20%) patients were in Partial-responder (PR), Stable-disease (SD) and Progressive-disease (PD) groups respectively. Pre-NACT (t0), average *ADC*, *D,D**& *f* in tumor volume were 1.36 ± 0.33 × $10^{-3}$ mm$^2$/s, 1.3 ± 0.3 × $10^{-3}$ mm$^2$/s, 28.44 ± 10.34 × $10^{-3}$ mm$^2$/s & 13.95 ± 2.83% respectively. Using ANOVA test, during NACT (t1, t2), *D*-variance* ($p$ = 0.038, 0.003) and *f-skewness* ($p$ = 0.03, 0.03) and at t2, *D*-entropy* ($p$ = 0.001) and *f-entropy* ($p$ = 0.002) and their Δ2 changes ($p$ = 0.001, 0.003) were statistically significant among response groups. At t1, *D*-variance* and *f-skewness* jointly showed AUC = 0.77 & 0.74 in classifying PR (Sensitivity = 73%; Specificity = 70%) and SD (Sensitivity = 74; Specificity = 75%) groups respectively in patient cohort. Δ1 & Δ2 changes of *D*-mean*, *D*-variance*, *D*-entropy* and *f-entropy* correlated well (0.5-0.6) with tumor-diameter and tumor-volume changes.

*Conclusions:* Quantitative IVIM parameters, especially *D** & *f* and their histogram analysis were informative and can be used as noninvasive surrogate markers for early response assessment during the course of NACT in Osteosarcoma.

## 1. Introduction

Osteosarcoma (OS) is the most common primary malignant bone tumor in children and adolescents and accounts for 3.4% of all childhood cancers [1]. Current treatment regimen for OS commonly involves neoadjuvant chemotherapy (NACT) [1]. Five-year disease-free survival rate for localized OS is 60–70%, whereas disease free survival rate is less than 20% in patients presenting with metastasis [1]. Monitoring treatment response is important during chemotherapy that might help in better and personalized therapeutic options improving overall therapeutic outcome [2–5]. RECIST1.1 is the currently accepted standard imaging criteria for non-invasive treatment response evaluation in solid tumors [6] that facilitates objective assessment of the changes in tumor burden in response to therapy.

Advanced functional MRI techniques like Diffusion weighted Imaging (DWI) [7–11], Perfusion MRI [12,13] and FDG-PET/CT [9]

* Corresponding author at: Centre for Biomedical Engineering, Indian Institute of Technology Delhi, Hauz Khas, New Delhi, India.
*E-mail address:* amit.mehndiratta@keble.oxon.org (A. Mehndiratta).

https://doi.org/10.1016/j.ejrad.2019.08.004
Received 5 April 2019; Received in revised form 4 August 2019; Accepted 8 August 2019

have been widely used for tumor characterization and treatment monitoring during NACT. While DWI uses water protons as endogenous contrast to assess diffusivity and tissue microstructure in tumor [7–11], perfusion MRI or FDG-PET/CT use exogenous contrast agents to assess tissue perfusion and metabolic activity in tumor [9,12,13] respectively. Therefore, DWI has the advantage over perfusion MRI and FDG-PET/CT that it does not involve any exogenous contrast agent. At the same time DWI might provide clinically useful information for prognostication.

Le Bihan et al. had shown that, at lower diffusion weighting factors (b-values ≤ 100 s/mm$^2$), fast attenuation of signal is contributed mostly by both, water diffusion in tissues and microcirculatory perfusion (*pseudo-diffusion*) within the capillary network, known as Intravoxel Incoherent Motion (IVIM) [14]. Quantitative IVIM analysis of DWI signal can separate the perfusion component from tissue diffusion and may help in better tissue characterization and treatment monitoring [15,16]. Thus, IVIM has been explored with promising results in characterizing and treatment monitoring of tumors in various organs like pancreas [17], prostate [18], cervix [19], breast [20,21], colon & rectum [22], head & neck [23] and nasopharynx [24,25] etc.

This study evaluates IVIM-diffusion-weighted MRI for tissue characterization and assessment of chemotherapy response in one of the rare solid tumors such as Osteosarcoma. The novelty of the study is also to perform IVIM analysis using one of the recently developed state-of-the-art techniques Bi-exponential (BE) model with adaptive Total Variation (TV) penalty function (BE + TV) [26] and evaluate the significance of various parameters in chemotherapy response evaluation using RECIST1.1 score as the reference standard. TV penalty function, widely used in image processing, is an image gradient based denoising method removing noise present in image regions and simultaneously preserving fine details and edges in the images [27]. Using DWI with low SNR, voxel-by-voxel parameter estimation by BE model may produce unreliable and noisy parametric maps [15]. As physiologically a spatial homogeneity in the tissue is expected, in BE + TV method, TV was incorporated into nonlinear least-square (NNLS) optimization to add a physiologically plausible spatial constraint to the BE model to iteratively reduce the non-physiological spatial inhomogeneity and spurious values during parameter estimation providing more reliable, qualitatively and quantitatively improved IVIM parametric maps [26].

## 2. Materials and methods

### 2.1. Patient cohort

This prospective study was performed from March, 2016 to March, 2019 under the Institutional Review Board approved protocol. Fifty-five patients (N = 55; Male:Female = 41:14; Age = 17.8 ± 5.5 years; Metastatic:localized = 29:26) with needle biopsy proven Osteosarcoma were enrolled for this study after obtaining written informed consent. Exclusion criteria were age below eight years and general contra-indication for MRI. Patients were planned for three cycles of NACT consisting of Cisplatin, Doxorubicin, Ifosfamide with/without high-dose of Methotrexate at every 3 weeks [28]. Total forty patients (N = 40; Male:Female = 30:10; Age = 17.7 ± 5.9 years; Metastatic:localized = 17:23) who completed three cycles of NACT, were further analyzed; fifteen patients could not complete NACT regimen due to death (n = 8/55, 15%), drop-out (n = 4/55, 7%) and early-surgery (n = 3/55, 5%) thus not included in final analysis. All patients had conventional type Osteosarcoma involving distal-femur (n = 18/40, 45%), proximal-tibia (n = 17/40, 43%), humerus (n = 3/40, 7%) and fibula (n = 2/40, 5%). All patients underwent conventional as well as diffusion-weighted MRI for evaluation of the primary tumor site and chest CT and bone scans for metastatic work-up. For each patient MRI was acquired at three time-points – pre-NACT (t0), after 1$^{st}$ NACT (t1, 2–3 weeks) and after 3$^{rd}$ NACT (t2, 8–9 weeks) and analyzed.

### 2.2. MRI acquisition protocol

MRI was acquired using a 1.5 T Philips Achieva® (Best, Netherland) MR scanner with phased-array surface coil or an extremity coil. A protocol including conventional T1-weighted (T1W), T2-weighted (T2W) with and without fat-saturation, and T2-weighted gradient-echo sequences was used. Patients underwent DWI using free breathing Spin Echo-Echo Planar imaging (SE-EPI) at 11 b-values (0, 10, 20, 30, 40, 50, 80, 100, 200, 400, 800 s/mm$^2$). DW sequence was acquired with TR/TE = 7541/67 msec, matrix-size = 192 × 192 and slice thickness/Gap = 5 mm/0.5 mm. The sequences acquired were based on the existing institutional protocol. The plane of acquisition and field-of-view were customized according to the tumor location and patient anatomy. The field-of-view ranged from 250 × 250 to 300 × 300 mm$^2$ and number of image slices ranged from 48 to 64.

### 2.3. RECIST score measurement

Region-of-interest (ROI) for tumor tissue was demarcated manually by a radiologist (> 10years of experience in cancer imaging), on each b = 800 DWI image-slice ($DWI_{800}$) with reference to the morphological T1W and T2W images at three time-points. Tumor-diameter (in cm) was measured at all three time-points using demarcated ROI having the maximum cross-sectional area of tumor. RECIST1.1 technique scores the amount of size changes in the soft tissue component of an osseous lesion during treatment as an indication of response [6]. Changes in tumor-diameter across time were calculated and NACT response evaluation was performed according to RECIST1.1 criteria [6]. Patients were classified as Complete-response (CR): total disappearance of tumor; Partial-response (PR): Minimum 30% decrease in tumor-diameter; Progressive-disease (PD): minimum 20% and 5 mm absolute increase in tumor-diameter; Stable-disease (SD): neither PR nor PD. Tumor-volume (in cc) was calculated separately at all the three time-points by selecting the tumor ROI across all slices. Relative percentage changes between time-points t0–t1 (Δ1) and time-points t0–t2 (Δ2) in tumor-diameter and tumor-volume were calculated.

### 2.4. Quantitative parameters estimation

Apparent diffusion coefficient (ADC) was calculated voxel-wise in tumor-volume at three time-points using mono-exponential fit at b-values ≥ 200 s/mm$^2$ as

$$S_b = S_{200}.\, e^{-b.ADC} \quad (1)$$

assuming perfusion effect is negligible at higher b-values (b ≥ 200 s/mm$^2$) [14,16,21–24,29].

IVIM parameters Diffusion-coefficient (*D*), Perfusion-coefficient (*D**) and Perfusion-fraction (*f*) were calculated in tumor-volume using state-of-the-art IVIM analysis method, Bi-exponential (BE) model with adaptive Total Variation (TV) Penalty function (BE + TV) [26]. The IVIM analysis BE model [14] is defined as:

$$S_b/S_0 = f\cdot e^{-b\cdot D^*} + (1-f)\cdot e^{-b\cdot D} \quad (2)$$

where, $S_0$ and $S_b$ are observed signals at diffusion weighting factor value of zero and b respectively. Non-linear least square optimization and image gradient based penalty Total Variation [27] was applied simultaneously in BE + TV method [26] to estimate the quantitative IVIM parameters. Goodness-of-fit ($R^2$) and Coefficient-of-variation (CV) were calculated as a measure of precision and reproducibility in parameter estimation respectively.

### 2.5. Histogram analysis

Histogram analysis was performed for functional parameters (*ADC, D, D** and *f*) in tumor-volume at three time-points. Five (n = 5)

quantitative parameters: mean, variance, skewness, kurtosis and entropy and their relative percentage changes (Δ1 (t1-t0) and Δ2 (t2-t0)) were calculated for each patient in tumor volume having averagely ~36420 ± 30543 voxels at all the time-points.

### 2.6. Statistical analysis

Statistical change in size and functional parameters between time-points t0–t1 and t0–t2 were tested for statistical significance ($p < 0.05$) using paired *t*-test. One-way ANOVA followed by Tukey post-hoc test was used to evaluate statistical significance ($p < 0.05$) in parameters and their Δ1 & Δ2 changes between response groups across three time-points. Performance of significant parameters in identifying NACT response was assessed using Receiver-operating-characteristic-curve (ROC) analysis at time-points t0 and t1 with Area-under-the-curve (AUC), Sensitivity (Sn), Specificity (Sp) and corresponding optimal Cut-off value. Correlation of Δ1 & Δ2 changes in tumor-diameter and tumor-volume with Δ1 & Δ2 changes in histogram of functional parameters were evaluated using Pearson-correlation-coefficient (R). Value of R may vary from -1 to 1; where R = ± 1 indicates perfect correlation and R = 0 indicates no correlation.

Evaluation of quantitative parameters and histogram analysis was performed using an in-house built toolbox in MATLAB® (MathWorks Inc., v2017, Philadelphia, USA) and statistical analysis were performed using SPSS 16.0 software.

## 3. Results

### 3.1. RECIST score assessment

According to RECIST1.1 criteria, 11 patients were categorized as PR (11/40, 27.5%), 21 as SD patients (21/40, 52.5%) and 8 as PD patients (8/40, 20%); whereas none of the patients were in CR category.

### 3.2. Tumor-diameter and tumor-volume

At t0, average tumor-diameter and tumor-volume in patient cohort were 9.76 ± 2.93 cm and 529.39 ± 520.95cc respectively. Average tumor-diameter and tumor-volume measured at three time-points among different response groups are summarized in Table1. In the course of NACT, while tumor-diameter in PR and SD groups broadly decreased, showing significant Δ2 decrement (PR: Δ1 = ~6 ± 17%, $p = 0.242$; Δ2 = ~35 ± 7%, $p < 10^{-6}$ and SD: Δ1 = ~0.5 ± 12%, $p = 0.662$; Δ2 = ~13 ± 7%, $p < 10^{-5}$); in PD group it showed increment (Δ1 = ~7 ± 8%, $p = 0.077$; Δ2 = ~15.89 ± 7%, $p < 10^{-4}$). During NACT, tumor-volume in PR group decreased (Δ1 = ~7 ± 56%, $p = 0.605$; Δ2 = ~56 ± 36%, $p = 0.002$) and in PD group it increased (Δ1 = ~23 ± 25%, $p = 0.065$; Δ2 = ~49 ± 55%, $p = 0.049$); while among SDs it was almost similar, showing no significant changes (Δ1 = ~24 ± 42%, $p = 0.304$; Δ2 = ~4 ± 46%, $p = 0.379$).

### 3.3. IVIM analysis

At t0, in patient cohort, mean *ADC, D, D* & f* values were $1.36 \pm 0.33 \times 10^{-3}$ mm$^2$/s, $1.3 \pm 0.3 \times 10^{-3}$ mm$^2$/s, 28.44 ± 10.34 × $10^{-3}$ mm$^2$/s and 13.95 ± 2.83% respectively. Mean $R^2$ value calculated for all measurement, was 0.97 ± 0.03 and mean CV were *ADC*:29.6 ± 9.2%, *D*:30.7 ± 10.1%, *D**:103.4 ± 23.2% and *f*:56.7 ± 12.9%. Average values of histogram parameters for all quantitative functional parameters across time-points among groups are presented in Table2.

In PR group, mean $ADC_{t0}$ ($1.3 \pm 0.24 \times 10^{-3}$ mm$^2$/s) was significantly lower($p < 10^{-3}$) than that of $ADC_{t1}$ ($1.68 \pm 0.32 \times 10^{-3}$ mm$^2$/s) or $ADC_{t2}$ ($1.69 \pm 0.3 \times 10^{-3}$ mm$^2$/s). Similarly, $D_{t0}$ ($1.24 \pm 0.25 \times 10^{-3}$ mm$^2$/s) was also significantly lower ($p < 10^{-3}$) than that of $D_{t1}$ ($1.6 \pm 0.3 \times 10^{-3}$ mm$^2$/s) or $D_{t2}$ ($1.61 \pm 0.26 \times 10^{-3}$ mm$^2$/s). Mean $D^*_{t0}$ ($27.69 \pm 9.62 \times 10^{-3}$ mm$^2$/s) among PRs was significantly higher ($p < 0.009$) than $D^*_{t1}$ ($18.16 \pm 5.86 \times 10^{-3}$ mm$^2$/s) as well as $D^*_{t2}$ ($17.54 \pm 10.85 \times 10^{-3}$ mm$^2$/s); whereas no significant difference ($p = 0.37$) was observed between $f_{t0}$ (13.4 ± 3.49%) and either $f_{t1}$ (12.31 ± 1.05%) or $f_{t2}$ (13.1 ± 1.46%). Fig. 1 illustrates a representative patient from PR group showing the respective changes in functional parameters.

In SD group, mean $ADC_{t0}$ ($1.42 \pm 0.39 \times 10^{-3}$ mm$^2$/s) was significantly lower ($p < 10^{-3}$) than that of $ADC_{t1}$ ($1.72 \pm 0.34 \times 10^{-3}$ mm$^2$/s) or $ADC_{t2}$ ($1.73 \pm 0.25 \times 10^{-3}$ mm$^2$/s). Similarly, $D_{t0}$ ($1.35 \pm 0.35 \times 10^{-3}$ mm$^2$/s) was also significantly lower ($p < 10^{-3}$) than $D_{t1}$ ($1.64 \pm 0.34 \times 10^{-3}$ mm$^2$/s) and $D_{t2}$ ($1.65 \pm 0.25 \times 10^{-3}$ mm$^2$/s). There was no significant change ($p = 0.16$) in average $D^*_{t0}$ ($29.39 \pm 11.09 \times 10^{-3}$ mm$^2$/s) and $D^*_{t1}$ ($24.3 \pm 9.7 \times 10^{-3}$ mm$^2$/s) among SDs; while $D^*_{t2}$ ($19.5 \pm 5.88 \times 10^{-3}$ mm$^2$/s) was significantly lower ($p = 0.001$) than $D^*_{t0}$. No significant difference ($p > 0.06$) was observed between $f_{t0}$ (13.4 ± 3.49%) and either $f_{t1}$ (12.31 ± 1.05%) or $f_{t2}$ (13.1 ± 1.46%) in SD group. Fig. 2 illustrates a representative patient from SD group showing the respective changes in functional parameters.

In PD group, average $ADC_{t0}$ ($1.34 \pm 0.28 \times 10^{-3}$ mm$^2$/s) was significantly lower ($p < 10^{-3}$) than that of $ADC_{t1}$ ($1.57 \pm 0.3 \times 10^{-3}$ mm$^2$/s) or $ADC_{t2}$ ($1.68 \pm 0.3 \times 10^{-3}$ mm$^2$/s). Similarly, $D_{t0}$ ($1.25 \pm 0.25 \times 10^{-3}$ mm$^2$/s) was significantly lower ($p < 10^{-3}$) than that of $D_{t1}$ ($1.5 \pm 0.27 \times 10^{-3}$ mm$^2$/s) or $D_{t2}$ ($1.61 \pm 0.26 \times 10^{-3}$ mm$^2$/s) among PDs. There was no significant change($p > 0.3$) in $D^*_{t0}$ ($27.22 \pm 10.58 \times 10^{-3}$ mm$^2$/s) and either $D^*_{t1}$ ($25.43 \pm 14.32 \times 10^{-3}$ mm$^2$/s) or $D^*_{t2}$ ($27.56 \pm 11.25 \times 10^{-3}$ mm$^2$/s) among PDs. Similarly, no significant change ($p > 0.4$) was observed

**Table 1**
Average tumor-diameter (cm) and tumor-volume (cc) measured among different response groups viz. Partial-responder (PR), Sable-disease (SD) and Progressive-disease (PD) at three time-points t0, t1 and t2 in the course of neoadjuvant chemotherapy.

| Response group | Tumor-diameter (cm) (Mean ± standard-deviation) | | | | | Tumor-volume (cc) (Mean ± standard-deviation) | | | | |
|---|---|---|---|---|---|---|---|---|---|---|
| | t0 | t1 | *p-value | t2 | #p-value | t0 | t1 | *p-value | t2 | #p-value |
| **PR** (n = 11) | 9.25 ± 2.02[#] | 8.59 ± 2.34 | 0.242 | 5.92 ± 1.42[#,†] | $< 10^{-6}$ | 525.79 ± 259.85[#] | 473.18 ± 392.34 | 0.605 | 163.32 ± 102.02[#,†] | 0.002 |
| **SD** (n = 21) | 10.43 ± 3.63[#] | 10.48 ± 3.81 | 0.662 | 9.06 ± 3.23[#,†] | $< 10^{-5}$ | 568.75 ± 676.47 | 650.72 ± 681.13 | 0.304 | 500.55 ± 395.8[†] | 0.379 |
| **PD** (n = 8) | 8.86 ± 1.81[#] | 9.49 ± 1.9 | 0.077 | 10.28 ± 2.22[#,†] | $< 10^{-4}$ | 440.84 ± 384.88[#] | 536.22 ± 423.23 | 0.065 | 650.93 ± 571.42[#,†] | 0.049 |
| †*p*-value | 0.363 | 0.285 | – | 0.002 | – | 0.851 | 0.694 | – | 0.022 | – |

[*] *p*-value according to paired *t*-test between time-points t0 and t1.
[#] *p*-value according to paired *t*-test between time point t0 and t2.
[†] *p*-value according to one-way ANOVA test among response groups at individual time points t0, t1 and t2.

**Table 2**
Histogram parameters of Apparent diffusion coefficient *(ADC)*, Diffusion-coefficient *(D)*, Perfusion-coefficient *(D*)* & Perfusion-fraction *(f)* observed in different response groups: Partial-responder (PD), Sable-disease (SD) and Progressive-disease (PD) at time points t0, t1 and t2 in the course of chemotherapy.

| | **PR** (n = 11) | | | **SD** (n = 21) | | | **PD** (n = 8) | | |
|---|---|---|---|---|---|---|---|---|---|
| | t0 | t1 | t2 | t0 | t1 | t2 | t0 | t1 | t2 |
| ***ADC*** | | | | | | | | | |
| Mean ($10^{-3}$xmm$^2$/s) | 1.3 ± 0.24*,# | 1.68 ± 0.32* | 1.69 ± 0.3# | 1.42 ± 0.39*,# | 1.72 ± 0.34* | 1.73 ± 0.25# | 1.34 ± 0.28*,# | 1.57 ± 0.3* | 1.68 ± 0.3# |
| Variance ($10^{-7}$) | 1.84 ± 0.61 | 1.88 ± 0.89 | 2.08 ± 0.91 | 2.12 ± 1.08 | 2.01 ± 0.92 | 2.31 ± 1.6 | 1.9 ± 0.94 | 1.9 ± 0.51 | 2.24 ± 1.22 |
| Skewness | 0.8 ± 0.43*,# | −0.17 ± 0.67* | −0.21 ± 0.51# | 0.63 ± 0.77*,# | −0.12 ± 0.76* | −0.36 ± 0.58# | 0.58 ± 0.47# | 0.28 ± 0.44 | 0.08 ± 0.29# |
| Kurtosis | 3.93 ± 1.17 | 3.73 ± 1 | 3.56 ± 1.05 | 4.88 ± 2.43 | 4.63 ± 1.58 | 3.96 ± 0.9 | 3.76 ± 0.59 | 3.45 ± 0.48 | 3.23 ± 0.39 |
| Entropy | 6.9 ± 0.22 | 6.94 ± 0.28 | 6.81 ± 0.33 | 6.81 ± 0.27 | 6.85 ± 0.29 | 6.88 ± 0.29 | 6.8 ± 0.25 | 6.9 ± 0.15 | 6.9 ± 0.22 |
| ***D*** | | | | | | | | | |
| Mean ($10^{-3}$xmm$^2$/s) | 1.24 ± 0.25*,# | 1.6 ± 0.3* | 1.61 ± 0.26# | 1.35 ± 0.35*,# | 1.64 ± 0.34* | 1.65 ± 0.25# | 1.25 ± 0.25*,# | 1.5 ± 0.27* | 1.61 ± 0.26# |
| Variance ($10^{-7}$) | 2.01 ± 1 | 1.82 ± 0.75 | 2.04 ± 0.9 | 2.1 ± 1.22 | 2.1 ± 1.03 | 2.05 ± 1.18 | 1.99 ± 0.95 | 2.02 ± 0.83 | 2.01 ± 1.14 |
| Skewness | 0.68 ± 0.38*# | −0.23 ± 0.69* | −0.2 ± 0.38# | 0.48 ± 0.75*,# | −0.1 ± 0.77* | −0.38 ± 0.57# | 0.64 ± 0.69# | 0.23 ± 0.52 | −0.05 ± 0.33# |
| Kurtosis | 4.25 ± 1.96 | 4.12 ± 1.25 | 4.01 ± 1.96 | 4.45 ± 1.52 | 4.83 ± 1.82 | 4.51 ± 1.41 | 5.03 ± 3.39 | 4.2 ± 1.83 | 3.44 ± 0.58 |
| Entropy | 6.67 ± .0.55 | 6.81 ± 0.28 | 6.79 ± 0.42 | 6.73 ± 0.29 | 6.83 ± 0.31 | 6.68 ± 0.39 | 6.72 ± 0.24 | 6.79 ± 0.21 | 6.82 ± 0.24 |
| ***D**** | | | | | | | | | |
| Mean ($10^{-3}$xmm$^2$/s) | 27.69 ± 9.62*,# | 18.16 ± 5.86* | 17.54 ± 10.85# | 29.39 ± 11.09# | 24.3 ± 9.7 | 19.5 ± 5.88# | 27.22 ± 10.58 | 25.43 ± 14.32 | 27.56 ± 11.25 |
| Variance ($10^{-4}$) | 6.27 ± 1.46*,# | 3.87 ± 1.52*,† | 3.64 ± 2.22#,† | 6.84 ± 1.93# | 5.79 ± 2.12† | 4.62 ± 1.5#,† | 5.8 ± 1.88 | 5.27 ± 2.09† | 6.74 ± 2.04† |
| Skewness | 0.84 ± 0.6*,# | 1.72 ± 0.87* | 1.71 ± 0.87# | 0.85 ± 0.91# | 1.17 ± 0.76 | 1.51 ± 0.65# | 0.8 ± 0.65 | 1.18 ± 1.06 | 0.92 ± 0.68 |
| Kurtosis | 2.86 ± 1.08 | 6.97 ± 6.59 | 6.84 ± 4.13 | 3.31 ± 3.04 | 3.87 ± 2.46 | 5.08 ± 3.45 | 2.99 ± 1.4 | 4.73 ± 3.5 | 3.04 ± 1.25 |
| Entropy | 9 ± 1.03# | 8.7 ± 0.84 | 7.73 ± 0.84.5#,† | 8.93 ± 0.92# | 8.92 ± 0.9 | 8.59 ± 0.82#,† | 8.78 ± 0.52# | 8.83 ± 0.68 | 9.09 ± 0.51#,† |
| ***f*** | | | | | | | | | |
| Mean (%) | 13.4 ± 3.49 | 12.31 ± 1.05 | 13.1 ± 1.46 | 14.06 ± 2.32# | 12.85 ± 2.15 | 12.49 ± 2.1# | 14.36 ± 3.04 | 14.44 ± 4.03 | 13.6 ± 2.84 |
| Variance ($10^{-3}$) | 6.72 ± 3.3* | 4.31 ± 1.4* | 5.4 ± 1.89 | 8.22 ± 7.94 | 6.56 ± 6.23 | 5.32 ± 2.97 | 8.44 ± 5.16 | 6.28 ± 4.02 | 5.98 ± 3.38 |
| Skewness | 1 ± 0.37 | 0.82 ± 0.28† | 0.83 ± 0.41† | 1.06 ± 0.36 | 1.15 ± 0.37† | 1.23 ± 0.45† | 0.97 ± 0.45 | 0.84 ± 0.4† | 1 ± 0.31† |
| Kurtosis | 5.03 ± 2.36 | 4.49 ± 1.27 | 4.61 ± 1.87 | 5.32 ± 1.67 | 5.92 ± 1.83 | 6.53 ± 2.22 | 4.73 ± 1.49 | 4.66 ± 1.98 | 5.25 ± 2.05 |
| Entropy | 8.99 ± 0.99# | 9.1 ± 0.72 | 8.08 ± 0.58#,† | 9 ± 0.77# | 8.81 ± 0.77 | 9.09 ± 0.89#,† | 8.91 ± 0.5*,# | 9.1 ± 0.52* | 9.22 ± 0.57#,† |

* Significantly change ($p < 0.05$) according to paired *t*-test between time point t0 and t1.
\# Significantly change ($p < 0.05$) according to paired *t*-test between time point t0 and t2.
† Significantly different ($p < 0.05$) according to one-way ANOVA test among groups at individual time points t0, t1 and t2.

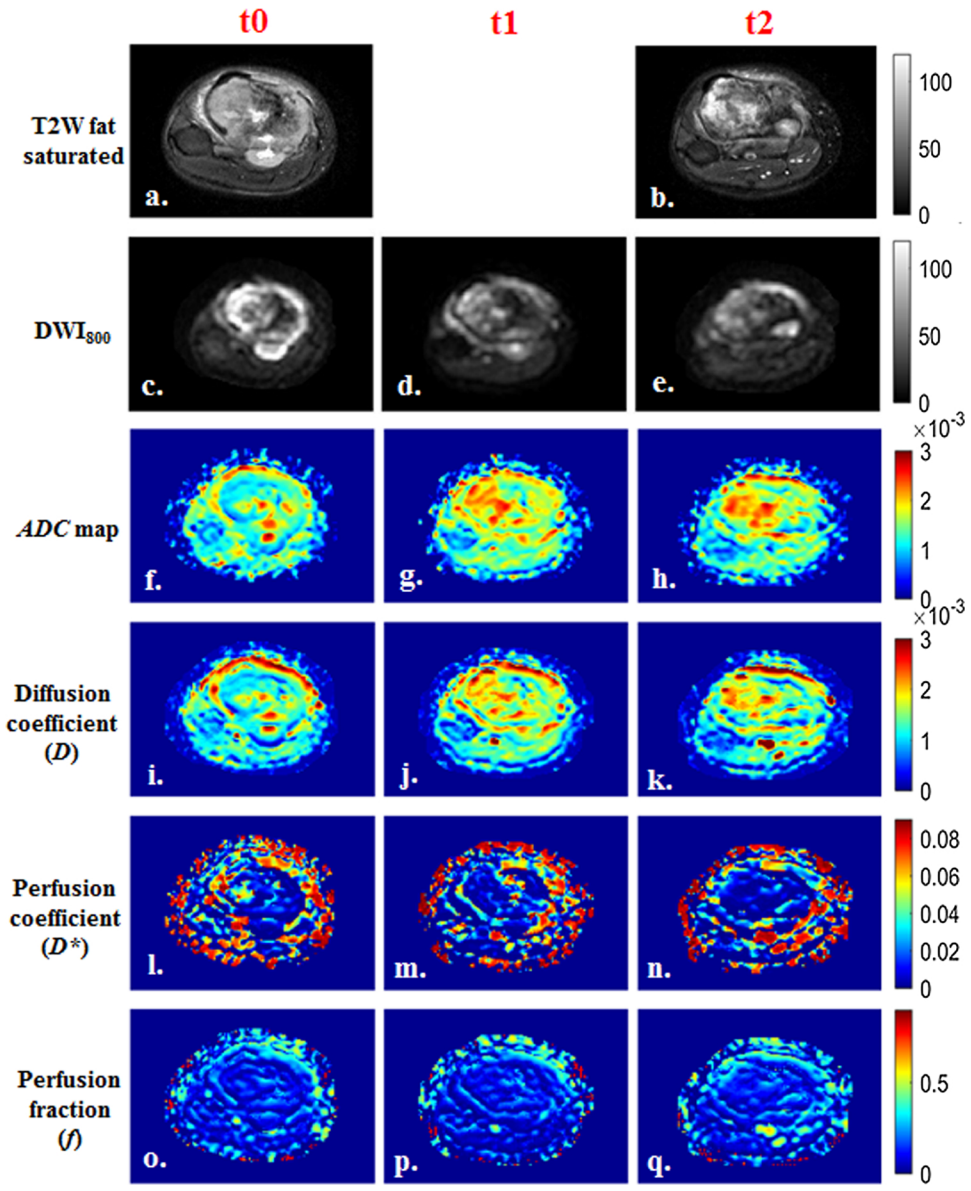


**Fig. 1.** a-q) Images of a representative patient from PR group (M, 16 years) with OS in left tibia and tumor-diameter was 6.6 cm, 6.5 cm and 4 cm at time points t0, t1 (Δ1:2% decrement) and t2 (Δ2:33% decrement) respectively. a,b) T2W fat-saturated image showing anatomical structure at time-points t0 and t2 respectively; c,d,e) DWI (b = 800 s/mm$^2$); f,g,h) Apparent diffusion coefficient (*ADC*); i,j,k) Diffusion coefficient (*D*); l,m,n) Perfusion coefficient (*D**); o,p,q) Perfusion fraction (*f*) at time points t0, t1 and t2 respectively. Both *ADC* & *D* in tumor demonstrated an increase; *D** showed a decrease; *f* did not show much difference in tumor ROI after chemotherapy.

in $f_{t0}$ (14.36 ± 3.04%) and either $f_{t1}$ (14.44 ± 4.03%) or $f_{t2}$ (13.6 ± 2.84%) in PD group. Fig. 3 illustrates a representative patient from PD group showing the respective changes in functional parameters.

### 3.4. Comparison of tumor size-parameters and functional-parameters among Response groups

According to paired *t*-test, after 1st cycle of NACT, *ADC-mean* & *D-mean* increased significantly ($p$ = 0.004, 0.006) and *ADC-skewness* & *D-skewness* decreased significantly ($p$ = 0.001, 0.002) among PR and SD groups except PDs. *D*-mean, D*-variance* & *f-variance* significantly reduced ($p$ = 0.01, 0.01, 0.04) and *D*-skewness* significantly ($p$ = 0.007) increased only among PG group; while SD and PD groups did not show any significant differences. According to ANOVA test, statistically significant ($p$ < 0.05) parameters and their Tukey post-hoc test among response groups are listed in Table3. Tumor-diameter and tumor-volume were significantly different among response groups ($p$ = 0.002, 0.022) only at t2. During NACT (t1, t2), *D*-variance* ($p$ = 0.038, 0.003 respectively) and *f-skewness* ($p$ = 0.03, 0.03 respectively) were significantly different among groups. Across t1 and t2, *D*-variance* was lower among PRs ((3.64–3.87 vs 4.62–5.79 and 5.27–6.74) x10$^{-4}$; $p$ = 0.038, 0.001) with significant Δ2 reduction (33%↓ vs, 9%↓, 4%↓; $p$ = 0.01) than PD and SD groups. At t1 and t2, *f-skewness* among PRs were lower than SD and PD groups (0.82-0.83 vs 1.15–1.23 & 0.84–1; $p$ = 0.03). After completion of NACT (t2), among PRs, *D*-entropy* ($p$ = 0.015, 0.002) and *f-entropy* ($p$ = 0.02, 0.003) were significantly lower with significant Δ2 reduction (9–13%↓ vs 2–3%↓, 3–4%↑; $p$ = 0.019, 0.001, 0.04, 0.003 respectively) than SDs and PDs groups. *ADC* and *D* showed no significant differences ($p$ > 0.05) among response groups.

Using ROC curve analysis, at t1, *D*-variance* (Sn:91%; Sp:67%; Cut-off: ≤ 0.49 × 10$^{-3}$) and *f-skewness* (Sn:73%; Sp:70%; Cut-off: ≤ 0.87) showed AUC of 0.75 and 0.69 respectively and in combination (*D*-variance* and *f-skewness*) showed Sn:73%, Sp:70% with AUC = 0.77 in classifying PR group among all patients. For classification of SDs from rest of the patients, *D*-variance* (Sn:58%; Sp:63%; Cut-off: ≤ 0.54 × 10$^{-3}$) and *f-skewness* (Sn:68%; Sp:75%; Cut-off: ≤ 0.96) individually showed AUC of 0.56 and 0.73 respectively and in combination (*D*-variance* and *f-skewness*) showed Sn:74%, Sp:75% with AUC = 0.74.

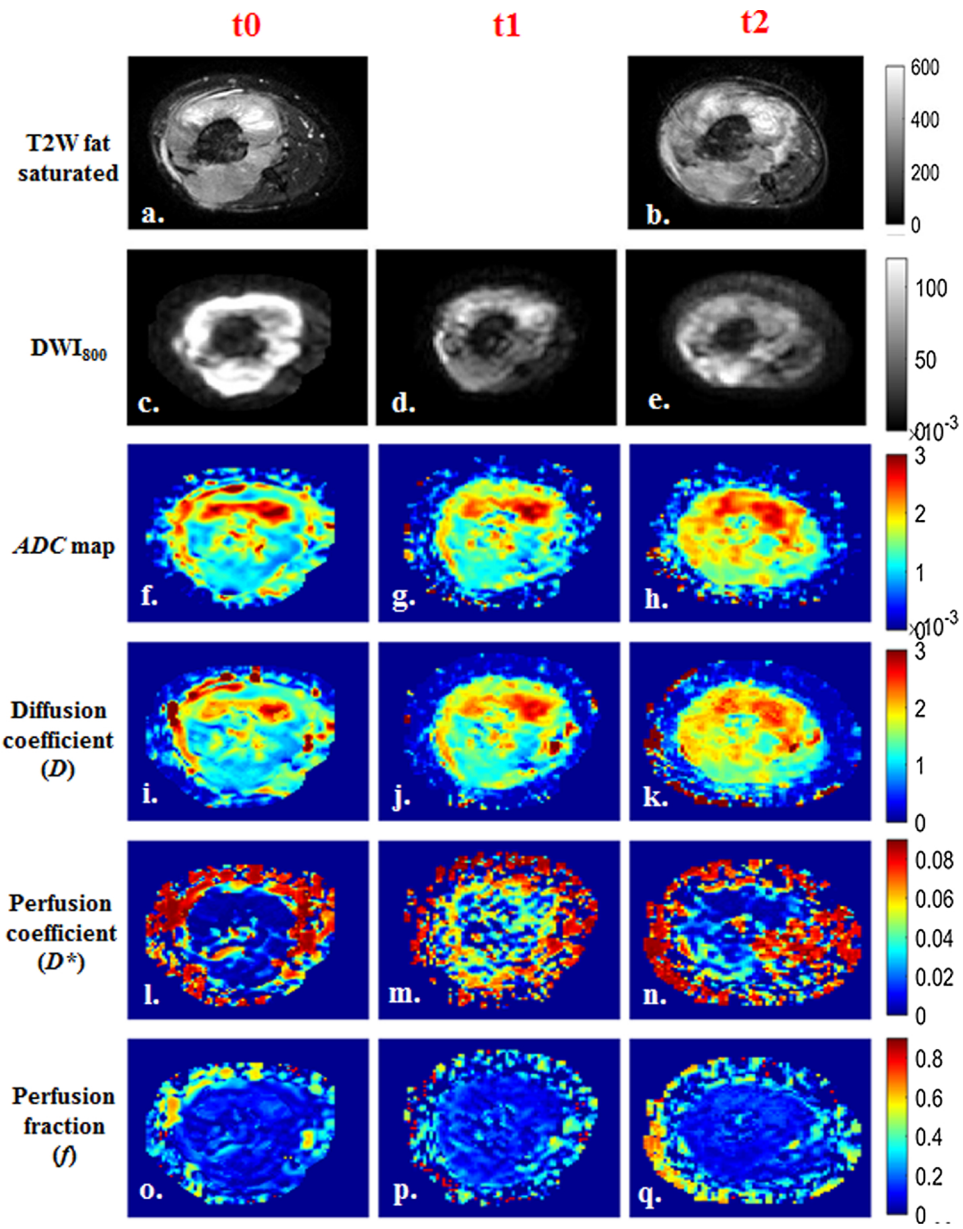


**Fig. 2.** a-q) Images of a representative patient from SD group (F, 15 years) with OS in left tibia in whom tumor-diameter was 8.5 cm, 10 cm and 7.2 cm at time points t0, t1 (Δ1:18% increment) and t2 (Δ2:15% decrement) respectively. a,b) T2W fat-saturated image showing anatomical structure at time-points t0 and t2 respectively; c,d,e) DWI ($b = 800\ s/mm^2$); f,g,h) Apparent diffusion coefficient (*ADC*); i,j,k) Diffusion coefficient (*D*); l,m,n) Perfusion coefficient (*D**); o,p,q) Perfusion fraction (*f*) at time points t0, t1 and t2 respectively. Both *ADC &D* in tumor demonstrated an increase; whereas *D** showed an increment at t1, followed by a decrease at t2; *f* did not show much difference in tumor ROI after chemotherapy.

### *3.5. Correlation between changes in tumor size-parameters and functional-parameters across time-points*

Δ1 and Δ2 changes among tumor-diameter and tumor-volume showed satisfactory correlation ($R = 0.54$ and 0.74 respectively). Pearson-correlation-coefficients for Δ1 and Δ2 changes between size-parameters and functional-parameters are presented in Table4. Δ1 of tumor-diameter and *ADC-mean* showed negative correlation ($R = -0.36$); while Δ2 of tumor-volume showed positive correlation with *ADC-entropy* and *D-variance* ($R = 0.4$). *D*-mean, D*-variance, D*-entropy* and *f-entropy* were positively correlated ($R \approx 0.39–0.64$) while *D*-skewness* and *D*-kurtosis* showed negative correlation ($R \approx -0.35–\ -0.44$) with both Δ1 and Δ2 changes of tumor-diameter and tumor-volume. Other functional-parameters showed poor correlation with tumor-diameter and tumor-volume changes.

## 4. Discussion

Non-invasive monitoring and assessment of treatment response in tumor early in the course of chemotherapy is very crucial as it may help to develop patient specific therapeutic options thus improving an overall therapeutic outcome. Novelty of the present study lies in performing quantitative analysis of IVIM-diffusion MRI in one of the rare solid tumors, Osteosarcoma and demonstrating efficacy of quantitative IVIM analysis using a recently developed technique BE + TV, in characterizing changes in tumor in the course of NACT. The study showed perfusion parameters of IVIM to be more accurate than diffusion parameters in characterizing and quantifying changes in Osteosarcoma early in the course of NACT. Moreover, histogram analysis revealed that, patients who responded better to NACT (PR group), had significant reduction in variability of perfusion parameters (*D** and *f*) early in the course of therapy. After 1st cycle of NACT, reduced *D*-variance* among PRs indicated that variability in micro-vascularization in tumor environment was significantly lower than SD & PD groups ($3.87 \times 10^{-4}$ vs $5.79 \times 10^{-4}$ and $5.27 \times 10^{-4}$ respectively, $p = 0.038$). In addition, significantly lower value of *f-skewness* among PRs (0.82 vs 1.15 and 0.84 respectively, $p = 0.03$), also indicated reduced perfusion fraction in tumor than in SD and PD groups after 1st cycle of NACT.

Diffusion and perfusion have been reported to provide effective non-

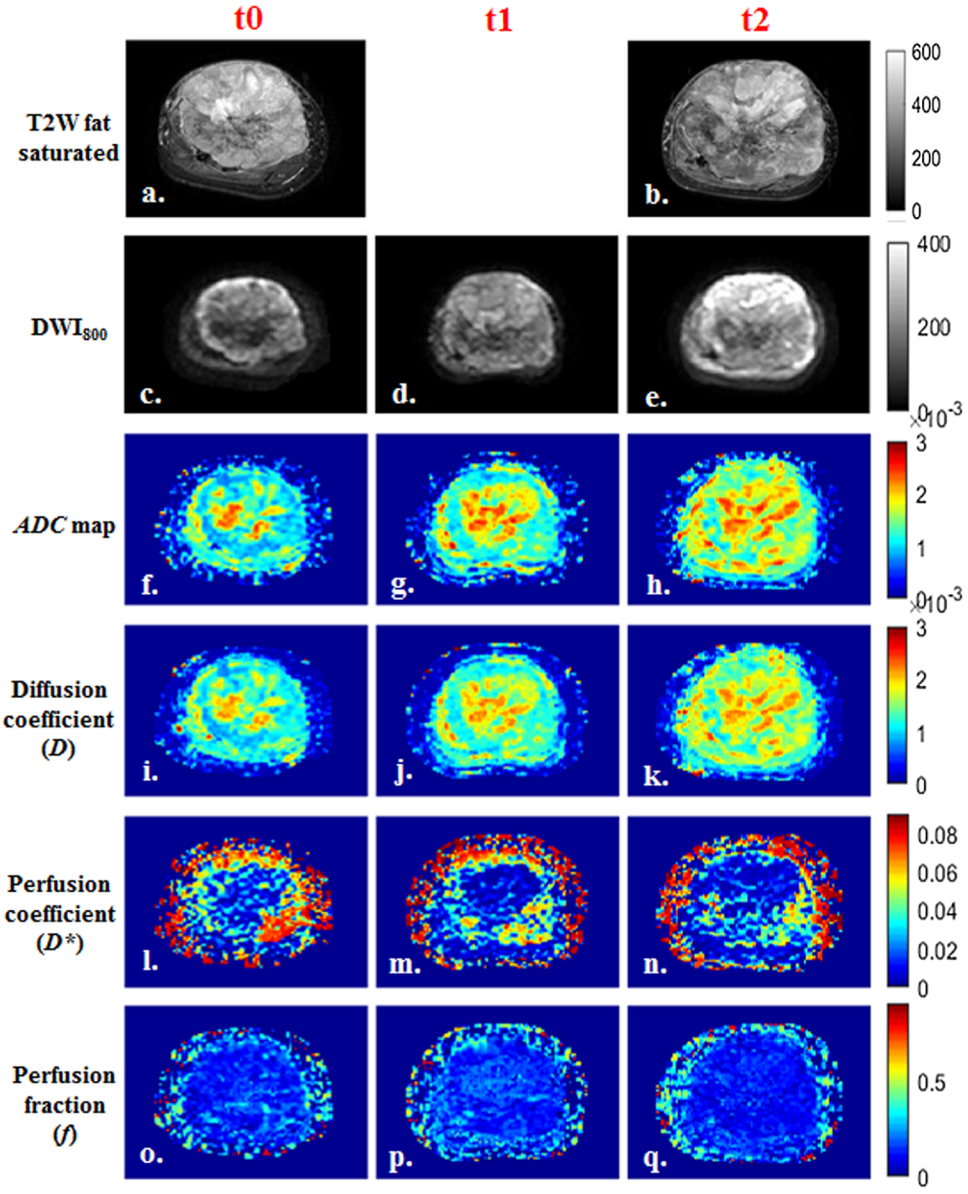


**Fig. 3.** a-q) Images of a representative patient from PD group (F, 30 years) with OS in left tibia in whom tumor-diameter was 10.4 cm, 12.6 cm and 11.5 cm at time points t0, t1 (Δ1:21% increment) and t2 (Δ2:11% increment) respectively. a,b) T2W fat-saturated image showing anatomical structure at time-points t0 and t2 respectively; c,d,e) DWI ($b = 800\,s/mm^2$); f,g,h) Apparent diffusion coefficient (*ADC*); i,j,k) Diffusion coefficient (*D*); l,m,n) Perfusion coefficient (*D**); o,p,q) Perfusion fraction (*f*) at time points t0, t1 and t2 respectively. Both *ADC&D* in tumor demonstrated an increase; whereas *D** showed a decrement after at t1, followed by an increase at t2; *f* did not show much difference in tumor ROI after chemotherapy.

**Table 3**
Statistically significant ($p < 0.05$) parameters according to ANOVA test at three time-points t0, t1 & t2 and their respective Tukey post hoc test among response groups. Statistically significant ($p < .05$) *p*-values are in bold.

| Time-points | Parameters | ANOVA test (*p*-value) | Tukey post-hoc test (*p*-value) | | |
|---|---|---|---|---|---|
| | | | PR vs SD | PR vs PD | SD vs PD |
| **t0** | – | – | – | – | – |
| **t1** | *D*-variance* | **0.038** | **0.038** | 0.29 | 0.809 |
| | *f-skewness* | **0.03** | **0.04** | 0.991 | 0.11 |
| **t2** | *D*-variance* | **0.003** | 0.348 | **0.003** | **0.026** |
| | *D*-entropy* | **0.001** | **0.015** | **0.002** | 0.283 |
| | *f-skewness* | **0.03** | **0.04** | 0.672 | 0.38 |
| | *f-entropy* | **0.002** | **0.02** | **0.003** | 0.343 |
| | Δ2 of *D*-variance* | **0.01** | 0.243 | **0.01** | **0.034** |
| | Δ2 of *D*-entropy* | **0.001** | **0.019** | **0.001** | 0.325 |
| | Δ2 of *f-entropy* | **0.003** | **0.04** | **0.003** | 0.206 |
| | Tumor-diameter | **0.002** | **0.003** | **0.001** | 0.606 |
| | Tumor-volume | **0.022** | 0.07 | **0.03** | 0.63 |

invasive bio-markers for NACT response in tumors like bone [7–13], nasopharyngeal [24], colorectal [22], head & neck [23] carcinoma etc. As cell-density and neovascularity may decrease after chemotherapy [2–5], extra-cellular space becomes capacious increasing tissue diffusion (*D*) and the micro-circulation in capillary network is reduced yielding a lower pseudo-diffusion (*D**) respectively. Our study showed an increase in *ADC* and *D* values in Osteosarcoma during course of NACT which is in agreement with previous studies [7–11]; though these were not statistically significant showing overlapping values among different response groups which has also been reported [7,10,11,23]. Further, a trend showing that lower pre-NACT *ADC* was associated with good prognosis [20,23], was also observed in our study where baseline *ADC and D* values among PRs were lower than SD and PD groups (ADC: $(1.3 \text{ vs } 1.42, 1.34) \times 10^{-3}\,mm^2/s$; D:$(1.24 \text{ vs } 1.35, 1.25) \times 10^{-3}\,mm^2/s$). Possibly, necrotic tumors with large extracellular space (with higher *ADC* and *D*) are often associated with poor response to therapy [8,23,24] due to hypoxia and tissue acidosis that leads to resistance to chemotherapy [2,30]. Our mean *ADC* values were consistent with previous studies involving Osteosarcoma [7–11] and observed lower *D* values compared to *ADC* due to pseudo-diffusion contamination was also in accordance with previous studies [19–21,24]. IVIM perfusion

**Table 4**
Pearson-correlation-coefficient (*R*) of relative percentage changes in Tumor-diameter and Tumor-volume across different time points (Δ1 & Δ2) with relative percentage changes of histogram parameters of diffusion and perfusion parameters *ADC*, *D*, *D** and *f* among all patients.

| | ***R*** with Tumor-diameter | | ***R*** with Tumor-volume | |
|---|---|---|---|---|
| | **Δ1** | **Δ2** | **Δ1** | **Δ2** |
| ***ADC*** | | | | |
| Mean Mean | −0.36* | −0.06 | −0.18 | −0.06 |
| Variance | 0.17 | 0.15 | 0.11 | 0.33 |
| Skewness | 0.10 | 0.06 | 0.13 | 0.12 |
| Kurtosis | 0.04 | −0.08 | 0.22 | 0.02 |
| Entropy | 0.17 | 0.27 | 0.13 | 0.40* |
| ***D*** | | | | |
| Mean | −0.27 | −0.07 | −0.05 | −0.07 |
| Variance | 0.09 | 0.18 | 0.10 | 0.40* |
| Skewness | 0.19 | 0.06 | 0.16 | 0.15 |
| Kurtosis | −0.02 | −0.09 | 0.20 | 0.03 |
| Entropy | 0.28 | −0.14 | 0.15 | −0.01 |
| ***D**** | | | | |
| Mean | 0.27 | 0.47* | 0.46* | 0.46* |
| Variance | 0.44* | 0.55* | 0.50* | 0.60* |
| Skewness | −0.33 | −0.31 | −0.39* | −0.35* |
| Kurtosis | −0.17 | −0.40* | −0.43* | −0.44* |
| Entropy | 0.39* | 0.61* | 0.56* | 0.64* |
| ***f*** | | | | |
| Mean | 0.23 | −0.19 | 0.33 | −0.09 |
| Variance | 0.24 | 0.14 | 0.28 | 0.32 |
| Skewness | 0.17 | 0.25 | −0.04 | 0.21 |
| Kurtosis | −0.07 | 0.11 | −0.05 | 0.20 |
| Entropy | 0.41* | 0.47* | 0.47* | 0.58* |

*Significant correlations ($p < 0.5$).

related parameters *D** and *f* correlates with the process of angiogenesis and reflects perfusion in micro-vasculature and vascular volume-fraction of tumor respectively. In the current study, Δ1 changes in *D*-mean, D*-variance* and *f-variance* showed significant reduction ($p = 0.009$, 0.009, 0.04) among PR group after 1st cycle of NACT, indicating reduced micro-vasculature in tumor, while SD and PD groups did not show any significant difference, which is in accordance with previous studies showing correlation between reduced perfusion level as the response to NACT in Osteosarcoma [12,13]. Perfusion fraction *f* did not show much changes during NACT among different response groups, although a higher baseline value of *f* was observed among poor response groups SD and PD than that of the PR group (~14% vs ~13% respectively). Similar observations have also been reported by Xiao et al. [24] and Hauser et al. [23] in nasopharyngeal carcinoma and head & neck squamous cell carcinoma respectively.

In this study, IVIM perfusion-related parameters were found informative in monitoring therapeutic effects of NACT in Osteosarcoma as these are sensitive to microcapillary perfusion and its changes during early phases of NACT. The ability of IVIM to characterize early changes in micro-vascular perfusion is highly relevant in this era of anti-angiogenic chemotherapy drugs which are known to reduce the vascularity without reducing the tumor size during the early part of NACT. Moreover, histogram analysis appears to be a useful statistical analysis technique as different parameters like variance, skewness and entropy were observed to be helpful in characterizing and quantifying changes in functional parameters (*ADC, D, D** and *f*) in Osteosarcoma in the course of NACT.

In evaluating *ADC*, as lower b-values are more sensitive to contributions from microcapillary perfusion, *ADC* was calculated by fitting the mono-exponential Eq. (1) for higher b-values ($b \geq 200\ s/mm^2$) in consensus with the recent literatures of IVIM analysis [14,16,21–24,29]. Commonly used IVIM analysis methodologies like BE model [14,18,19,29], segmented-BE techniques with 2-parameter fitting [21,22,24,25,29], and 1-parameter fitting [17,20,23,29] optimize the signal fitting at each voxel independently, overlooking the spatial context that results in high noise obscuring features of interest in the estimated parametric images [15]. Thus, adding a physiologically plausible spatial constraint to the existing BE model is expected to provide a more reliable parametric estimation. Therefore, our recently developed regularized IVIM parameter estimation method BE + TV [26] has been used to achieve the desired reliability and reproducibility. As spatial homogeneity in the tissue is expected physiologically, image gradient based penalty Total Variation [27] was incorporated into the standard NNLS optimization of BE model to develop BE + TV method [26]. Total variation penalty function is an image gradient based denoising method and has advantages over other smoothening techniques of removing noise present in flat regions and simultaneously preserving the fine details and edges in the images. BE + TV applied NNLS optimization for data fitting and the desired spatial homogeneity and noise reduction in the parametric images were achieved by updating the parametric images (*D, D*, f*) iteratively with the adaptive TV penalty, at each iteration of NNLS optimization. Thus, NNLS error and TV penalty reduction were adaptively and simultaneously balanced as solution progressed to the reliable direction reducing non-physiological spatial inhomogeneity and noise. Using simulation data and empirical clinical data of bone tumors like Osteosarcoma and Ewing's sarcoma, BE + TV have shown quantitatively and qualitatively improved IVIM parameter estimation than existing BE (CV improvement: 30–50% in *D* and 50% in *D** & *f*) and segmented-BE techniques (CV improvement: 7–23% in *D** and 26–30% in *f*) [26]. In this study $R^2$ and CV values for evaluated IVIM parameters were comparable with previous studies [24,25,29]. Although, relatively higher CVs were observed for *D** and *f* compared to *ADC* and *D* that might be due to highly heterogeneous angiogenic environment in Osteosarcoma reflecting large standard-deviation in *D** and *f* values.

There are few limitations in our study. This study mainly evaluated the chemotherapeutic changes in Osteosarcoma with respect to the RECIST1.1 criteria based on MRI measurements. Evaluation with histopathological assessment of necrosis might have been useful. However, objective of the study was to evaluate IVIM parameters for non-invasive monitoring of treatment response only. Second, perfusion imaging would have been beneficial to characterize angiogenesis changes after treatment, however we could not do contrast MRI as it was more expensive and time consuming considering the fact that our study protocol involved three time point imaging for each patient. Third, long term disease-free survival outcome has not been evaluated as the focus was on characterizing early changes in osteosarcoma treated with NACT and its correlation with response. Although, a long term follow-up study would have been beneficial, we could not do it because of limited resources which is one of the limitations of this study. Fourth, due to small number of patients in different histological subtypes of Osteosarcoma and their complex changes after NACT, a high variability can be seen in the evaluated parameters that does not allow a strong conclusion to be made. Finally, the sample size of this prospective study was relatively small that could result in a statistical bias. Thus, in future, studies with large cohort and multi-centric data with standardized and optimized MRI protocol and long-term survival follow-up are needed.

## 5. Conclusion

IVIM perfusion-related parameters (*D*, f*) were shown to be useful to differentiate responders from non-responders early in the course of NACT in patients with Osteosarcoma. Patients with higher relative percentage change in IVIM parameters during the course of NACT had a better prognosis. Therefore, quantitative IVIM analysis with BE + TV technique is an effective methodology for monitoring and evaluating chemotherapy response in patients with Osteosarcoma.

## Funding

This research did not receive any specific grant from funding agencies in the public, commercial, or not-for-profit sectors.

## Declaration of Competing Interest

We wish to confirm that there are no known conflicts of interest associated with this publication and there has been no significant financial support for this work that could have influenced its outcome.

## Acknowledgements

Authors would like to thank the Patients for their consensual participation in this study. Authors would also like to acknowledge the support of nursing staff and MRI technicians in patient recruitment and data acquisition respectively, during the study period from March, 2016 to March, 2019.

## References

[1] D.S. Geller, R. Gorlick, Osteosarcoma : a review of diagnosis, management, and treatment strategies, Clin. Adv. Hematol. Oncol. 8 (2010) 705–718.
[2] A.K. Raymond, S.P. Chawla, C.H. Carrasco, A.G. Ayala, C.V. Fanning, B. Grice, T. Armen, C. Plager, N.E. Papadopoulos, J. Edeiken, Osteosarcoma chemotherapy effect: a prognostic factor, Semin. Diagn. Pathol. 4 (1987) 212–236.
[3] N. Jaffe, Osteosarcoma: review of the past, impact on the future. The American experience, in: N. Jaffe, O.S. Bruland, S. Bielack (Eds.), Pediatr. Adolesc. Osteosarcoma, Springer US, Boston, MA, 2010, pp. 239–262, , https://doi.org/10.1007/978-1-4419-0284-9_12.
[4] C.M. Coffin, A. Lowichik, H. Zhou, Treatment effects in pediatric soft tissue and bone tumors: practical considerations for the pathologist, Am. J. Clin. Pathol. 123 (2005) 75–90, https://doi.org/10.1309/H0D4VD760NH6N1R6.
[5] K.A. Janeway, H.E. Grier, Sequelae of osteosarcoma medical therapy : a review of rare acute toxicities and late eff ects, Lancet Oncol. 11 (2010) 670–678, https://doi.org/10.1016/S1470-2045(10)70062-0.
[6] E.A. Eisenhauer, P. Therasse, J. Bogaerts, L.H. Schwartz, D. Sargent, R. Ford, J. Dancey, S. Arbuck, S. Gwyther, M. Mooney, L. Rubinstein, L. Shankar, L. Dodd, R. Kaplan, J. Lacombe, J. Verweij, New response evaluation criteria in solid tumours: revised RECIST guideline (version 1.1), Eur. J. Cancer 45 (2009) 228–247, https://doi.org/10.1016/j.ejca.2008.10.026.
[7] T. Kubo, T. Furuta, M.P. Johan, M. Ochi, N. Adachi, Value of diffusion-weighted imaging for evaluating chemotherapy response in osteosarcoma : a meta-analysis, Mol. Clin. Oncol. 7 (2017) 88–92, https://doi.org/10.3892/mco.2017.1273.
[8] C. Wang, L. Du, M. Si, Q. Yin, L. Chen, M. Shu, F. Yuan, X. Fei, X. Ding, Noninvasive assessment of response to neoadjuvant chemotherapy in osteosarcoma of long bones with diffusion-weighted imaging : an initial in vivo study, PLoS One 8 (2013) e72679, , https://doi.org/10.1371/journal.pone.0072679.
[9] B.H. Byun, C. Kong, I. Lim, C.W. Choi, W.S. Song, W.H. Cho, D. Jeon, J. Koh, S. Lee, S.M. Lim, Combination of 18F-FDG/CT and diffusion-weighted MR imaging as a predictor of histologic response to neoadjuvant chemotherapy : preliminary results in osteosarcoma, J. Nucl. Med. 54 (2013) 1–8, https://doi.org/10.2967/jnumed.112.115964.
[10] J. Bajpai, S. Gamnagatti, R. Kumar, V. Sreenivas, M.C. Sharma, K.S. Alam, R. Shishir, A. Malhotra, R. Safaya, S. Bakhshi, Role of MRI in osteosarcoma for evaluation and prediction of chemotherapy response : correlation with histological necrosis, Pediatr. Radiol. 41 (2011) 441–450, https://doi.org/10.1007/s00247-010-1876-3.
[11] K. Oka, T. Yakushiji, H. Sato, Y. Yamashita, H. Mizuta, The value of diffusion-weighted imaging for monitoring the chemotherapeutic response of osteosarcoma : a comparison between average apparent diffusion coefficient and minimum apparent diffusion coefficient, Skelet. Radiol. 39 (2010) 141–146, https://doi.org/10.1007/s00256-009-0830-7.
[12] H.J. van der Woude, J.L. Bioem, L. Verstraete, a Nooy, Osteosarcoma and Ewing' s sarcoma after neoadjuvant chemotherapy : value of dynamic imaging in detecting, Am. J. Roentgenol. 165 (1995) 593–598.
[13] P. Amit, A. Malhotra, R. Kumar, L. Kumar, D.K. Patro, S. Elangovan, Evaluation of static and dynamic MRI for assessing response of bone sarcomas to preoperative chemotherapy: correlation with histological necrosis, Indian J. Radiol, Imaging. 25 (2015) 269–275, https://doi.org/10.4103/0971-3026.161452.
[14] D. Le Bihan, E. Breton, D. Lallemand, M.L. Aubin, J. Vignaud, M. Laval-Jeantet, Separation of diffusion and perfusion in intravoxel incoherent motion MR imaging, Radiology. 168 (1988) 497–505, https://doi.org/10.1148/radiology.168.2.3393671.
[15] D. Koh, D.J. Collins, M.R. Orton, Intravoxel incoherent motion in body diffusion-weighted MRI: reality and challenges, AJR Am. J. Roentgenol. 196 (2011) 1351–1361, https://doi.org/10.2214/AJR.10.5515.
[16] M. Iima, D. Le Bihan, Clinical intravoxel incoherent motion and diffusion MR imaging: past, present, and future, Radiology. 278 (2016) 13–32, https://doi.org/10.1148/radiol.2015150244.
[17] A. Lemke, F.B. Laun, M. Klau, T.J. Re, D. Simon, S. Delorme, L. Schand, B. Stieltjes, Differentiation of pancreas carcinoma from healthy pancreatic tissue using multiple b-values: comparison of apparent diffusion coefficient and intravoxel incoherent motion derived parameters, Invest. Radiol. 44 (2009) 769–775, https://doi.org/10.1097/RLI.0b013e3181b62271.
[18] H. Shinmoto, C. Tamura, S. Soga, E. Shiomi, N. Yoshihara, T. Kaji, R.V. Mulkern, An intravoxel incoherent motion diffusion-weighted imaging study of prostate cancer, Am J Roentgenol. 199 (2012) W496–W500, https://doi.org/10.2214/AJR.11.8347.
[19] X. Li, P. Wang, D. Li, H. Zhu, L. Meng, Y. Song, L. Xie, J. Zhu, T. Yu, Intravoxel incoherent motion MR imaging of early cervical carcinoma: correlation between imaging parameters and tumor-stroma ratio, Eur. Radiol. 28 (2018) 1875–1883, https://doi.org/10.1007/s00330-017-5183-3.
[20] R. Bedair, A.N. Priest, A.J. Patterson, M.A. McLean, M.J. Graves, R. Manavaki, A.B. Gill, O. Abeyakoon, J.R. Griffiths, F.J. Gilbert, Assessment of early treatment response to neoadjuvant chemotherapy in breast cancer using non-mono-exponential diffusion models: a feasibility study comparing the baseline and mid-treatment MRI examinations, Eur. Radiol. 27 (2017) 2726–2736, https://doi.org/10.1007/s00330-016-4630-x.
[21] C. Liu, C. Liang, Z. Liu, S. Zhang, B. Huang, Intravoxel incoherent motion (IVIM) in evaluation of breast lesions : comparison with conventional DWI, Eur. J. Radiol. 82 (2013), https://doi.org/10.1016/j.ejrad.2013.08.006 e782–e789.
[22] V. Granata, R. Fusco, O. Catalano, S. Filice, M.D. Amato, G. Nasti, A. Avallone, F. Izzo, A. Petrillo, Early assessment of colorectal cancer patients with liver metastases treated with antiangiogenic drugs : the role of intravoxel incoherent motion in diffusion-weighted imaging, PLoS One 10 (2015) e0142876, , https://doi.org/10.1371/journal.pone.0142876.
[23] T. Hauser, M. Essig, A. Jensen, F.B. Laun, M. Münter, K.H. Maier-Hein, Prediction of treatment response in head and neck carcinomas using IVIM-DWI : evaluation of lymph node metastasis, Eur. J. Radiol. 83 (2014) 783–787, https://doi.org/10.1016/j.ejrad.2014.02.013.
[24] Y. Xiao, J. Pan, Y. Chen, Y. Chen, Z. He, X. Zheng, Intravoxel incoherent motion-magnetic resonance imaging as an early predictor of treatment response to neoadjuvant chemotherapy in locoregionally advanced nasopharyngeal carcinoma, Med. 94 (2015) e973, https://doi.org/10.1097/MD.0000000000000973.
[25] N. Fujima, D. Yoshida, T. Sakashita, A. Homma, A. Tsukahara, Y. Shimizu, K.K. Tha, K. Kudo, H. Shirato, Prediction of the treatment outcome using intravoxel incoherent motion and diffusional kurtosis imaging in nasal or sinonasal squamous cell carcinoma patients, Eur. Radiol. 27 (2017) 956–965, https://doi.org/10.1007/s00330-016-4440-1.
[26] E.B. Kayal, D. Kandasamy, K. Khare, J.T. Alampally, S. Bakhshi, R. Sharma, A. Mehndiratta, Quantitative analysis of intravoxel incoherent motion (IVIM) diffusion MRI using total variation and Huber penalty function, Med. Phys. 44 (2017) 5489–5858, https://doi.org/10.1002/mp.12520.
[27] L.I. Rudin, S. Osher, E. Fatemi, Nonlinear total variation based noise removal algorithms, Phys. D. 60 (1992) 259–268, https://doi.org/10.1016/0167-2789(92)90242-F.
[28] The ESMO / European Sarcoma Network Working Group, Bone sarcomas : ESMO clinical practice guidelines for diagnosis, treatment and follow-up, Ann. Oncol. 23 (2012), https://doi.org/10.1093/annonc/mds254 vii100–vii109.
[29] E.M. Meeus, J. Novak, S.B. Withey, N. Zarinabad, H. Dehghani, A.C. Peet, Evaluation of intravoxel incoherent motion fitting methods in low-perfused tissue, J. Magn. Reson. Imaging 45 (2017) 1325–1334, https://doi.org/10.1002/jmri.25411.
[30] J.L. Tatum, G.J. Kelloff, R.J. Gillies, Hypoxia : importance in tumor biology, noninvasive measurement by imaging, and value of its measurement in the management of cancer therapy, Int. J. Radiat. Biol. 82 (2006) 699–757, https://doi.org/10.1080/09553000601002324.